Bulletin of Geophysics and Oceanography Vol. XX, n. X, pp. XXX-XXX; Xxxxx 20xx
DOI 10.4430/bgo00538

Ionospheric total electron content response before and after the 7.7 magnitude earthquake in Myanmar on 28 March 2025

M.S. Paudel[1, 2], S. Chudal[2], B.D. Ghimire[3] and N.P. Chapagain[4]

[1] *Central Department of Physics, Institute of Science of Technology, Tribhuvan University, Nepal*
[2] *Department of Physics, Tri-Chandra Multiple Campus, Tribhuvan University, Nepal*
[3] *Department of Physics, St. Xavier's College, Tribhuvan University, Nepal*
[4] *Department of Physics, Amrit Campus, Tribhuvan University, Nepal*

(Received: 23 July 2025; accepted: 23 June 2026; published online: 12 November 2026)

ABSTRACT In this study, we try to uncover the seismo-ionospheric coupling mechanism associated with the latest earthquake in Myanmar with 7.7 magnitude which occurred on 28 March 2025 at 22.011°N, 95.936°E, at 12:50 PM Myanmar Standard Time. The ionospheric total electron content (*TEC*) is derived from the pseudo-range measurements obtained from a dual frequency global navigation satellite system (GNSS) receiver. The ionospheric *TEC* is studied over a 40-day timeframe (i.e. from 3 March to 12 May 2025) using data from nine GNSS stations within and outside the earthquake preparation zone. The running quartile-based thresholds are used to identify the *TEC* anomalies. The anomalous *TEC* variations are observed from 12 days before to 4 days after the earthquake in geomagnetically calm conditions (*Dst* > -50nT and *Kp* < 5). The spatiotemporal variation of the observed anomalies is cross-examined using the *TEC* global ionospheric map. The west-to-east shift of the *TEC* anomaly and morphological change in the equatorial ionisation anomaly (EIA) profile is observed before earthquakes. The observed *TEC* anomalies and EIA dynamics near the epicentre indicate the seismo-ionospheric coupling prior to the Myanmar earthquake.

Key words: *TEC*, Myanmar M7.7 earthquake, EIA profile, seismo-ionospheric coupling.

1. Introduction

The emission of a pre-seismic electromagnetic wave as a precursor of an earthquake has been studied by many authors (Hayakawa and Molchanov, 2002; Hayakawa, 2006, 2007). The lithosphere-atmosphere-ionosphere coupling (LAIC) model, associated with the earthquake based on the three possible observables (namely chemical, acoustic waves, and electromagnetic waves), was well described by Hayakawa (2006). The enhancement of the electric field in the atmosphere and its consequences in the ionosphere were significantly studied using the ground-based and space-based measurements focused on a specific region. The anomalies in the critical frequency of the F2 layer of the ionosphere, based on the quartile-based statistical analysis, was studied by Chen *et al*. (1999) and Liu J.Y. *et al*. (2000, 2006). The development of the global positioning system (GPS) and later global navigation satellite system (GNSS) enable the continuous observation of the Earth and measurement of the ionospheric total electron content

© 2026 - The Author(s)

(*TEC*) (Liu *et al.,* 1996). In recent years, there has been rapid growth in the study of ionospheric *TEC* as a precursor of earthquakes using the GPS/GNSS-based measurements which are able to detect both positive and negative *TEC* anomalies from a few days up to weeks before the day of the earthquake. To describe how the ionospheric *TEC*, together with the various atmospheric/climatic parameters, is connected with seismic activity, a unified model on LAIC was presented by Pulinets and Ouzounov (2011), based on previous research (Pulinets *et al.*, 1997, 1999, 2004, 2007; Liu *et al.*, 2004, 2006, 2010; Ouzounov *et al.*, 2006, 2007).

In recent years, the study of ionospheric *TEC* obtained from ground-based GNSS stations as well as from the global ionospheric map (GIM) was able to provide evidence of the precursor before large earthquakes, i.e. those with magnitude greater than 5.0, by identifying spatiotemporal variations in *TEC* anomalies. The timing of the observed *TEC* anomalies varied before the earthquakes. Tariq *et al.* (2019) declared anomalies in ionospheric *TEC* three days before the *M*7.8 earthquake on 25 April 2015 in Nepal, five days before the *M*7.3 earthquake on 12 May 2015 in Nepal, and 10 days before the *M*7.3 earthquake in 2017 on the Iran–Iraq border, using GNSS station data in Pakistan. For the *M*7.8 earthquake of 25 April 2015 in Nepal, Ghimire and Chapagain (2022) studied ionospheric *TEC* anomalies one and nine days before the earthquake using the multiple GNSS stations in Nepal. Kiyani *et al.* (2020) studied the *M*8.2 earthquake in Fiji in 2018 and noticed anomalies in *TEC* five to ten days before and five days after the earthquake. Nayak *et al.* (2023) detected the anomalies six days before the *M*6.8 earthquake in Morocco whereas for the *M*7.8 earthquake in New Zealand 60% of the *TEC* anomalies was detected 14–15 days before and 30–40% two to three days before the earthquake (Simha *et al.*, 2023). In most of the studies, the *TEC* anomalies were observed during the daytime but at different UTC hours. In some studies, it has been reported that the enhancement in *TEC* anomalies is accompanied by the equatorial ionisation anomaly (EIA) (Ryu *et al.,* 2014).

In low-latitude regions, the *TEC* anomaly is associated with the EIA. Pulinets and Legenka (2002) suggested the modification of the *TEC* profile in the EIA prior to the large earthquakes either by increasing or decreasing it in relation to the undisturbed condition. Moreover, the distortion of the EIA crest and, at times, the disappearance of one of the crests were noticed. The physical mechanism for observed anomalies in case of low-latitude earthquake is described by Pulinets (2012).

On 28 March 2025, an *M*7.7 earthquake hit Mandalay, Myanmar at 22.011° N, 95.936° E, at 12:50 PM Myanmar Standard Time (MMT; UTC+6:30) and its aftershock of *M*6.7 after 12 minutes at 21.698° N, 95.969° E. The depth of both the main shock and the aftershock are 10.0 km (USGS, n.d.). The epicentre of this earthquake lies near the boundary of the Indian and Eurasian plate. Historically, this region has experienced relatively less seismic activity, with no earthquakes with magnitude greater than 7.0 recorded in Myanmar over the past three decades. The most recent *M*7.0 earthquake occurred in January 1991 at 23.613° N, 95.901° E, near Mogok, Myanmar. From 1970 to 1988, four earthquakes occurred near the border of Myanmar, of which two in India and two in China. Recently, from 2011 to 2016, four earthquakes were recorded in this region, with magnitudes between 6.8 and 6.9.

This work aims to study the ionospheric *TEC* anomalies before and after the *M*7.7 Myanmar earthquake in the 40-day timeframe, from 25 days before to 15 days after the earthquake, together with the geomagnetic and solar indices. Our aim is to explore the possible seismo-ionospheric coupling mechanism associated with this earthquake. The details of the data sources and method of analysis are provided in Section 2, the results and discussion are presented in Section 3, and the conclusions are summarised in Section 4.

2. Materials and methods

2.1. Data sources

In this work, we have used data from different sources, which are explained here in brief. The information on the earthquake magnitude, epicentre location, depth, and time were taken from the United States Geological Survey (USGS) website (USGS, n.d.). The pseudo-range from ground-based dual frequency receivers at various GNSS stations within the radius of the earthquake preparation zone (EPZ) was taken from the website of the University NAVSTAR consortium (UNAVCO, n.d.). The ionospheric slant *TEC* (*STEC*) and vertical *TEC* (*VTEC*) were calculated using these data following Seemala (2023). The name of the GNSS stations and their latitude, longitude, and altitude are provided in Table 1. At a few stations, data were unavailable on some days; for example, on 25 and 26 March and 8 to 13 April at station CUSV, on 18 March at station HYDE, and on 14 and 21 March and 4 to 5 April at station HKSL. The distance between the epicentre and the GNSS station was estimated using the Vincenty (1975) formula, which is based on the World Geodetic System 1984 (WGS-84) coordinate system and is widely used in geodesy.

The geomagnetic indices including disturbance storm time (*Dst*) index, planetary *K*-index (*Kp* index), Auroral Electrojet (*AE*) index, Solar Flux F10.7 cm (*F*10.7), and Sunspot number (*SSN*) were obtained from the Omni-web data explorer (NASA Space Physics Data Facility, n.d. 2). The information of the geomagnetic quiet days (Q-days) and disturb days (D-days) was obtained from the International Service of the Geomagnetic Indices (ISGI, n.d.). It provides five D-days and ten Q-days for each month, ranked from the most effective to less effective. We studied *VTEC* from 3 March to 12 April 2025. In March, the D-days were days 26, 13, 22, 27, and 12, while the Q-days were days 3, 2, 31, 30, 20, 6, 29, 10, 11, and 16. Similarly, in April, the D-days were days 16, 5, 21, 4, and 15, whereas the Q-days were days 28, 25, 1, 29, 26, 23, 27, 17, 30, and 7.

The GIM-TEC, with a spatial resolution of 2.5°×5.0° along latitude × longitude and produced by the International GNSS Service working group and available through the NASA website (NASA Space Physics Data Facility, n.d. 1), was also used in this study. Data with two-hour temporal resolution were used to construct the *TEC* map and data with one-hour temporal resolution were used to study the EIA dynamics. The GIM-TEC data covers ±90° along the latitude and ±180° along the longitude so that there are 71×73 grid points in total. We studied the region nearby the epicentre, from 20° S to 35° N and 50° E to 130° E (22×16 grids). This spatial resolution is sufficient

Table 1 - Country, latitude, longitude, altitude, and distance of the GNSS stations from the epicentre. The negative altitude indicates the stations are below the mean sea level.

Station Number	GNSS station	Country	Latitude (°N)	Longitude (°E)	Altitude (m)	Distance from epicentre (km)
1	PUST	Bangladesh	22.465	90.383	-37.8	574.62
2	KHL2	Bangladesh	22.802	89.533	-36.0	665.02
3	PD32	Bangladesh	22.505	89.436	-48.1	672.16
4	SNT1	Bangladesh	22.252	89.805	-37.5	685.37
5	CUSV	Thailand	13.736	100.534	74.3	1037.18
6	KUGE	Nepal	27.618	85.539	1,465.1	1220.12
7	HKSL	Hong Kong	22.372	113.928	95.3	1854.72
8	HYRD	India	17.417	78.551	441.7	1890.75
9	IISC	India	13.021	77.570	843.7	2186.44

to analyse the variation of the *TEC* covering the EPZ. The extra latitudinal region to the south is included to cover the magnetically conjugate region of EIA. The earthquake shake map and the EPZ with its radius and ground-based GNSS stations can be seen in Fig. 1.

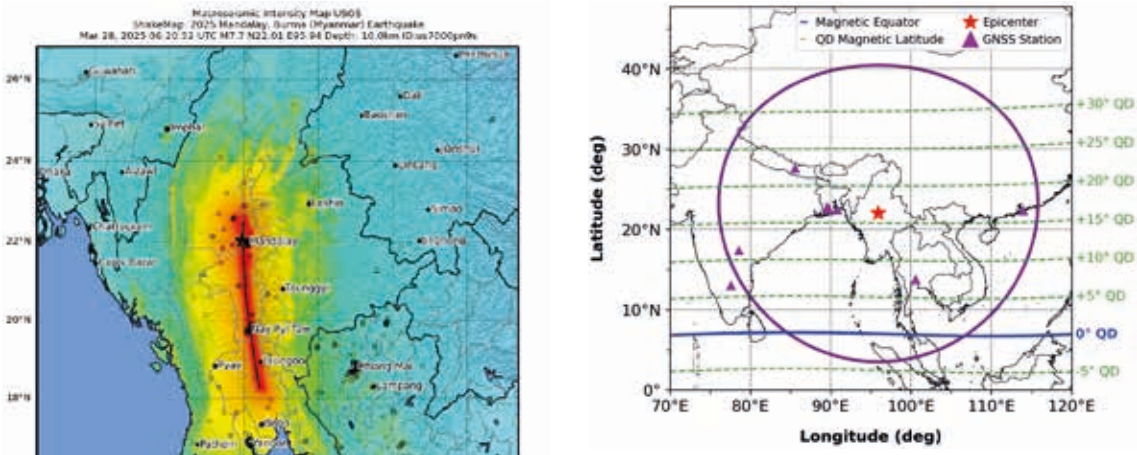


Fig. 1 - Left: colour map showing the effect of earthquake shaking caused by Myanmar *M*7.7 earthquake (Source: USGS). Right: the geographical view around the epicentre of the Myanmar earthquake. The circle represents the region of the EPZ and the dotted curved lines represent the quasi-dipole geomagnetic latitudes; the blue line is the geomagnetic equator.

The GNSS stations are divided into four categories on the basis of the distance from the epicentre, their latitude, and EPZ. Namely: i) stations close to the epicentre and at the EIA north crest, which are PUST, KHL2, PD32, and SNT1; ii) stations far from the epicentre and at the EIA north crest, which are KUGE and HKSL; iii) stations far from the epicentre and between the EIA north crest and the trough region, which are CUSV and HYDE; iv) the station outside the EPZ and between the EIA north crest and the trough region, which is IISC. This classification facilitates the identification and isolation of the observed *TEC* anomalies.

2.2. Methods

2.2.1. Estimation of *STEC* and *VTEC*

Ionospheric *TEC*, defined as the line integral of the electron density along a path through the ionosphere over a unit cross-sectional area, provides the quantitative measure of ionisation level in the ionosphere. Being a dispersive medium, the refractive index of the ionosphere is frequency dependent, which is inversely proportional to the square of the GNSS frequency. In the ionosphere, GNSS signals experience a path delay due to refraction, which is frequency dependent. Ionospheric *TEC* can be estimated from the pseudo-range of the GNSS signal at two frequencies f_1 (1575.42MHz) and f_2 (1227.6 MHz). The *TEC* along the path followed by signal is

known as the *STEC*, which is estimated as:

$$STEC = \frac{1}{40.3}\left(\frac{f_1^2 f_2^2}{f_2^2 - f_1^2}\right)[P_1 - P_2 - c(DCB^s + DCB_r)] \quad (1)$$

where, P_1 and P_2 are the pseudo-range of the GNSS signal at frequency f_1 and f_2, DCB^s and DCB_r are the differential code bias for the satellite and receiver, respectively (Seemala, 2023).

The *VTEC* is obtained using the following formula:

$$VTEC = STEC \times \sqrt{1 - \left(\frac{R\ cosZ}{R + H}\right)^2} \quad (2)$$

where *R* is the radius of the Earth equal to 6378 km, *Z* is the elevation angle of the satellite with respect to the receiver, and *H* (350 km) is the height of the ionospheric pierce point based on the single layer model (Seemala, 2023). The elevation angle is chosen to be greater than 20° during the estimation of the *VTEC*.

The *TEC* is measured in *TEC* units (TECU), where one TECU equals 10^{16} electron/m^2. The GPS-*TEC* analysis program software by Seemala (n.d.) was used for the estimation of the *STEC* and *VTEC*.

2.2.2. Earthquake preparation zone

According to the empirical relation given by Dobrovolsky *et al.* (1979), the radius of the region around the epicentre of the earthquake, where the precursor in atmosphere and ionosphere parameter are likely to be observed, can be determined as:

$$R = 10^{0.43M} \quad (3)$$

where *M* is the earthquake moment magnitude and *R* is the radius in km. For the *M*7.7 Myanmar earthquake the radius is 2046.44 km.

Table 1 summarises the latitude, longitude, altitude, and epicentral distances of the GNSS stations used in this study. To assess anomaly differences outside the EPZ, data from GNSS station IISC were also included in the study.

2.2.3. Upper and lower bound for *VTEC*

The identification of the anomalous value of the *VTEC* is one of the important aims of this work. The *VTEC* value is low at early morning and takes its peak at noon, starting again to decrease at night time. In this work, we analyse the data from 3 March to 12 April. The analysis is based on the hourly averaged data. In several previous studies (Liu J.Y. *et al.,* 2000, 2010; Le *et al.,* 2011; Liu J. *et al.,* 2016; Tariq *et al.,* 2019), a 15-day dataset was used to estimate the running median (M), lower quartile (Q_1) and upper quartile (Q_3). In contrast, Shah and Jin (2018) estimated these values using the data of the previous 30 days. This year (2025) belongs to the solar maximum year, therefore, to obtain more consistent results we used 30-day data to create a lower bound (*LB*) and upper bound (*UB*) for the *VTEC* for the 31st day. M, Q_1, and Q_2 are estimated from the dataset of the previous 30 days in the same hour and *LB* and *UB* are estimated using the following formula (Chen *et al.*, 1999; Liu J.Y. *et al.*, 2000, 2006, 2010):

$$LB = M - K(M - Q_1) \tag{4}$$

$$UB = M + K(Q_3 - M) \tag{5}$$

The value of *K* is chosen to be 2.0 so as to cover the range $M \pm 1.34\sigma$, where σ is the standard deviation. Whenever the *VTEC* values fall beyond either the lower or upper bound, they can be considered anomalous with approximately 82% confidence level. This is based on the assumptions that the *VTEC* pattern follows the normal distribution (Neter *et al.,* 1988; Chen *et al.,* 1999; Liu J.Y. *et al.,* 2000).

The difference between the *VTEC* and either the *UB* or *LB*, represented as the *TEC* deviation (*dTEC*), is also computed to quantify the anomaly in *VTEC* value. The *dTEC* is defined as follows (Liu J.Y. *et al*., 2009; Shah and Jin, 2018);

$$\begin{aligned} dTEC &= VTEC - UB; \quad \text{if } VTEC > UB \quad \text{(positive value)} \\ &= 0; \quad \text{if } LB < VTEC < UB \\ &= VTEC - LB; \quad \text{If } VTEC < LB \quad \text{(negative value)} \end{aligned} \tag{6}$$

The persistence of an anomaly over successive hours is crucial for identifying potential anomalous days before and after an earthquake. Le *et al.* (2011) considered a minimum six consecutive hour anomaly as a criterion, although the threshold used for the *LB* and *UB* were less stringent. In this work, a day is classified as a potential anomaly day if the anomaly persists for more than three consecutive hours and is observed simultaneously at all the stations under study. In stations CUSV, HKSL, and HYDE, data are missing on few days. However, this does not significantly affect the estimation of the *dTEC* and detection of the anomalies because the remaining data are sufficient to estimate the desired parameters.

2.2.4. Estimation of deviation in *TEC* for GIM-TEC data

GIM-TEC data, with a spatial resolution of 2.5° in latitude and 5.0° in longitude and a temporal two-hour resolution, were used in this study. For each grid cell and every two-hour interval, a 30-day running median of *TEC* was calculated. The *dTEC* for a given day (31st day) was, then, obtained by subtracting the corresponding 30-day running median from the observed *TEC* value. The resulting *dTEC* maps were used to analyse the spatiotemporal evolution of *TEC* anomalies within the periphery of the EPZ.

3. Results and discussion

3.1. Time series of VTEC *from GNSS stations*

The variation in the *VTEC* in the 40-day timeframe, from 3 March to 12 April is studied. Since, there is no significant anomaly before 12 March and after 8 April, the temporal variation of *VTEC*, together with the *UB* and *LB*, is presented only between 12 March and 8 April as shown in Figs. 2 to 4. Whenever, the *VTEC* value increases above the *UB* or decreases below the *LB*, it is recognised as a positive or negative anomaly, respectively. The positive and negative anomalies

are represented by the blue and red dots in the graph. In each graph, the *dTEC* value is plotted simultaneously in the lower panel. The geomagnetic conditions are represented by different colours: D-days red, Q-days green, and normal days black.

For nearby stations, in Fig. 2, the trend of positive and negative anomalies is identical. The positive anomalies are observed on 16, 20, 22, 23, 26, 27, 28, and 29 March and 1 April. The negative anomalies are observed on 13 and 25 March and 5 and 8 April. 13, 22, 26, and 27 March and 5 April were characterised by moderate geomagnetic disturbances (*Dst* < -50 nT). The anomalies observed on these days are, therefore, attributed to the geomagnetic disturbance rather than to the Myanmar earthquake. The variation of the geomagnetic and solar indices within the 40-day timeframe, from 3 March to 12 April, is presented in Section 3.2.

The trend of the anomalies observed from nearby stations is different compared to the distant stations. The anomalies observed in distant stations are very important to isolate the true anomaly associated with the earthquake. The negative anomaly on 8 April is absent in stations CUSV and HKSL but present in stations HYDE and IISC. The anomaly present outside and absent within the EPZ can be removed from the list of anomalous days potentially associated with the earthquake. The remaining anomaly days as a potential earthquake precursor are 16, 20, 23, 25, 28, and 29 March and 1 April.

On 16 March, strong anomaly is observed in all stations except in HYDE and HKSL and on 20 March anomaly is absent only in station HKSL. On 23, 28, and 29 March anomaly is absent only in station HYDE. Although stations CUSV and HYDE are located within similar latitudinal range in the EPZ, an anomaly is observed at station CUSV on that day when no anomaly appears at station HYDE. This difference may be attributed to the closer proximity of station CUSV to the epicentre and the associated tectonic fault line.

The negative anomaly observed on 25 March is most prominent among all other days because: i) it is observed from all stations within the EPZ; ii) absent in stations outside the EPZ; iii) the anomaly is stronger at stations near the epicentre and with similar latitudinal positions (PUST, KHL2, PD32, SNT1, HKSL), and weak in those distant (KUGE, HYDE). Kiyani *et al.* (2020) demonstrated during the 2018 *M*8.2 Fiji earthquake that the timing of *TEC* anomaly varied at GNSS stations depending on the geographic latitude and epicentral distance. Similarly, the station-specific anomalies observed in this study may be attributed to variations in distance and latitude. The anomalies observed from stations nearby the epicentre are more prominent and trustworthy in the context of the seismo-ionospheric coupling mechanism (Ghimire and Chapagain, 2022). It is evident that the timing and magnitude of *TEC* anomalies vary across different stations. The maximum *dTEC* value among all stations and the corresponding time is presented in Table 2. Furthermore, since the earthquake epicentre is located in the low-latitude region, the study of the morphological change in the EIA profile before the earthquake is more important. This aspect is discussed in the following section.

3.2. Geomagnetic condition

The geomagnetic and solar indices are studied to identify whether the ionospheric *TEC* is affected by space weather conditions, especially in this timeframe. The variation of the *Dst* index, *Kp* index, *AE* index, *F*10.7 index, and *SSN*, from 3 March 2025 to 12 April 2025, can be seen in Fig. 5. The different level of the geomagnetic storm and solar activity is separated by horizontal lines (Gonzalez *et al.*, 1994; Tapping, 2013). Days 13, 22, 26, and 27 March belong to the geomagnetic D-days, when an anomaly in ionospheric *TEC* can be observed and the *Dst* and *Kp* indices cross the threshold values for moderate geomagnetic storm (*Dst* < -50 nT, *Kp* > 5). On other anomalous

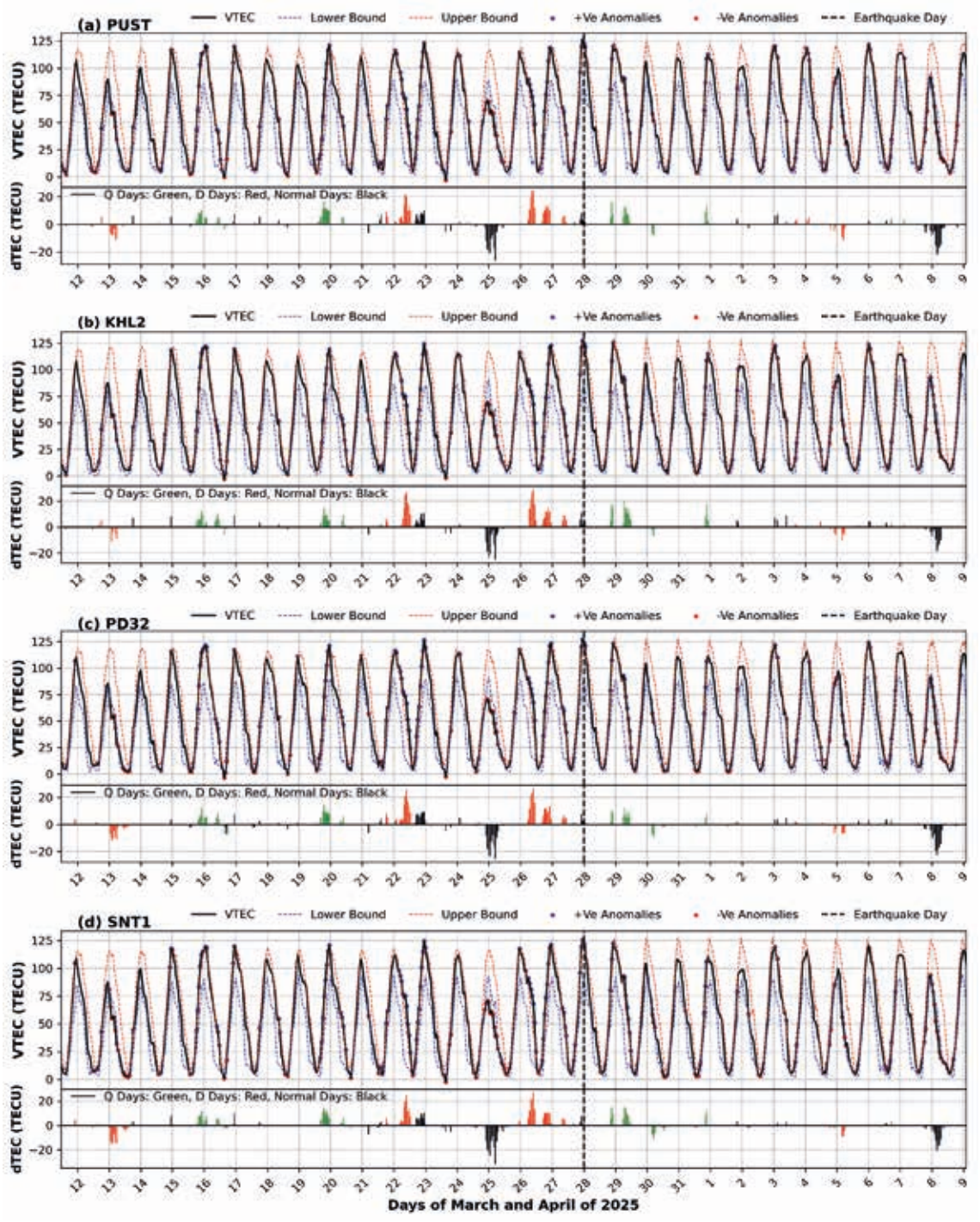


Fig. 2 - The variation of *VTEC* together with *LB* and *UB* from 12 March to 8 April for nearby GNSS stations: a) PUST, b) KHL2, c) PD32, and d) SNT1, respectively from top to bottom. In each figure; lower panel shows the histogram of *dTEC* corresponding to positive and negative anomaly. The colour in histogram corresponds to geomagnetic disturb (red), quiet (green) and normal (black) days. The vertical line shows the earthquake day.

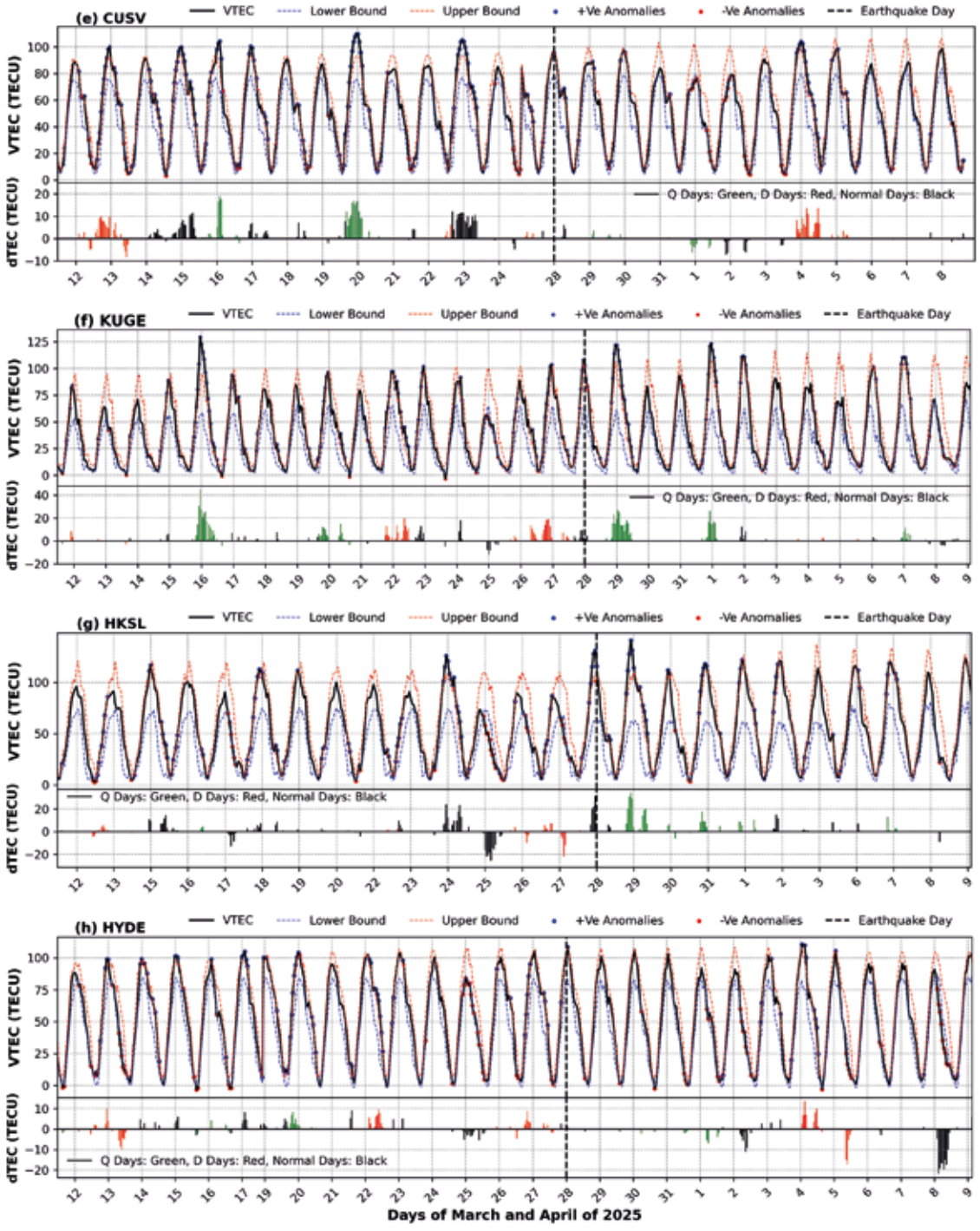


Fig. 3 - The variation of *VTEC* together with *LB* and *UB* from 12 March to 8 April for distant GNSS stations: e) CUSV, f) KUGE, g) HKSL, and h) HYDE respectively from top to bottom. Stations KUGE and HKSL lie on the EIA north crest, CUSV and HYDE, lie between the EIA north crest and trough.

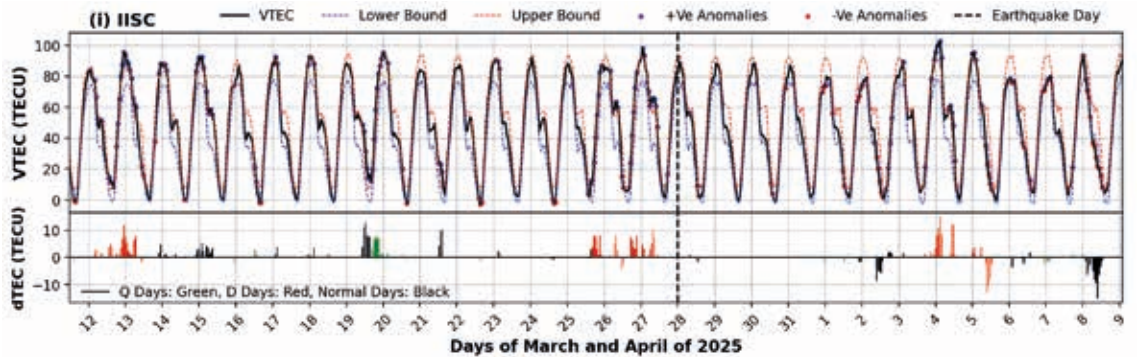


Fig. 4 - The variation of *VTEC* together with *LB* and *UB* from 12 March to 8 April for GNSS station IISC, which lies outside the EPZ.

days, we have also examined the hourly values of the *Kp* and *Dst* indices and *VTEC* in each hour and noted the maximum value of the days, as presented in Table 2.

Higher values for the *AE* index, i.e. above 1000 nT, are observed on 12 and 26 March and on 4 and 12 April when the *Dst* index reduces below -50nT. However, as the epicentre of the Myanmar earthquake belongs to the low-latitude region, we can safely ignore its effect on the *TEC* anomalies. The *F*10.7 index and *SSN* remained high throughout the 40-day window due to the solar cycle maxima in 2025. On 17 March, the *F*10.7 index and *SSN* both crossed 200 units but no *TEC* anomalies were noticed. Being in the solar maxima time, the overall value of *TEC* is higher but solar flux and *SSN* has no effect on the *TEC* anomaly. The *TEC* anomalies observed on Q-days and normal days must be associated with the earthquake-induced disturbance in the global electric circuit (GEC), which is discussed further in the following section.

Table 2 - The maximum value of *dTEC* over all stations, maximum value of *Kp* index and minimum value of *Dst* index on the anomaly days is given in table.

	16 March	**20 March**	**23 March**	**25 March**	**28 March**	**29 March**	**1 April**
dTEC (TECU), UTC, Station	45.23, 06:00, KUGE	16.92, 08:00, KUGE	12.94, 06:00, KUGE	-32.07, 13:00, SNT1	31.41, 07:00, HKSL	34.36, 06:00, HKSL	17.85, 05:00, KHL2
Kp Index ×10, UTC	33, 12:00	23, 21:00	40, 00:00	40, 18:00	40, 21:00	33, 03:00	20, 18:00
Dst Index (nT), UTC	-23, 12:00	-20, 00:00	- 41, 00:00	-43, 23:00	-27, 22:00	-15, 03:00	6, 13:00

3.3. Spatiotemporal variation of dTEC *from the GIM-TEC*

The GIM-TEC taken from the international GNSS service is used to cross-validate the anomalies in the *VTEC* observed from ground-based GNSS stations as well as for the spatiotemporal distribution of the *dTEC* within the EPZ. To create the *dTEC* map, we used GIM-TEC data with a temporal resolution of two hours, so as to obtain 12 separate maps for each day. Each map covers from latitude 20° S to 35° N and longitude: 50° E to 130° E, so that both crests of the EIA can be clearly seen. The map is studied from 16 March to 1 April. It should be noticed that

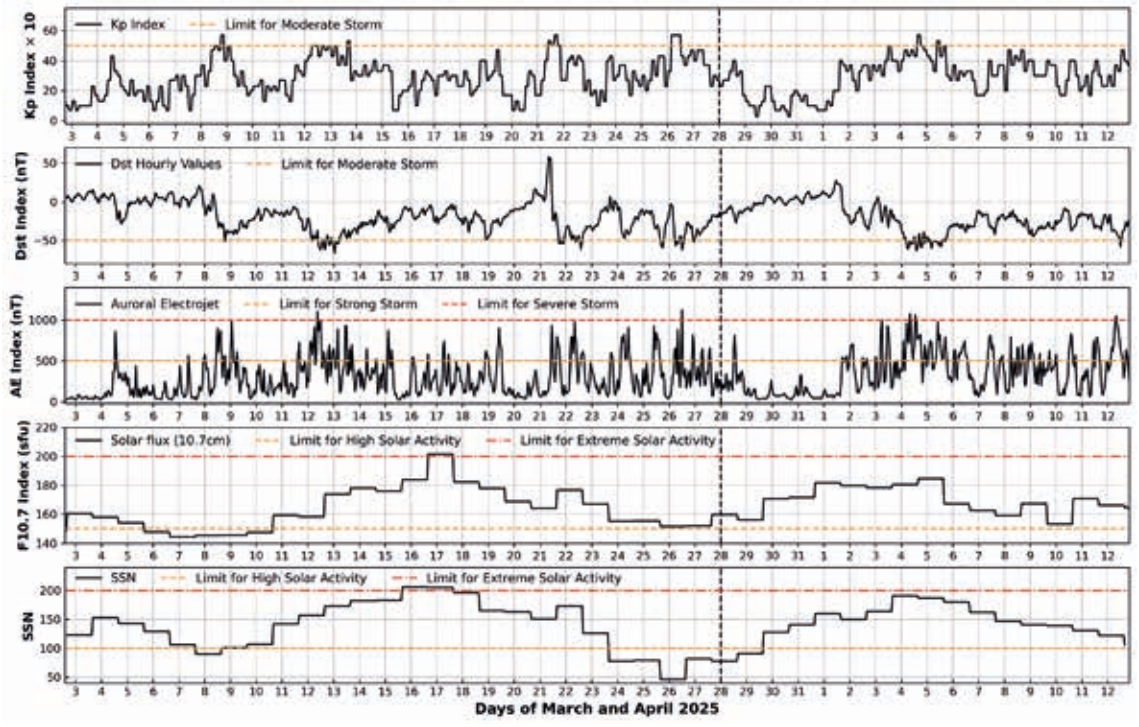


Fig. 5 - The variation of geomagnetic and solar indices; *Kp* index, *Dst* index, *AE* index, *F*10.7 index and *SSN* from top to bottom, from 3 March to 12 April 2025. Horizontal lines show the limiting level for geomagnetic and solar activity, vertical line on 28 March represents the earthquake day.

the EPZ belongs to the low-latitude region, so it lies in the EIA regions. The analysis of the EIA indicates that the *TEC* begins to increase around 5:00 UTC (11:30 LT), reaches its maximum value between 08:00 and 09:00 UTC (between 14:30 and 15:30 LT), and generally persists until approximately 18:00 UTC (00:30 LT). The anomaly in *dTEC* is analysed considering the position of the EIA with different UTCs and LTs. The *dTEC* map for the days on which the EIA exhibited a normal rise-and-settle trend is not presented in this study. The selected map can be seen in Figs. 6 and 7.

A rigorous observation of the GIM-TEC map of *dTEC* data shows the sudden appearance of the EIA maxima towards the west from epicentre on 17 and 23 March from 06:00 to 10:00 UTC (12:30 to 16:30 LT). In the same hours, the EIA is observed in the eastern side from the epicentre on 24 March. The longitudinal shifts of the EIA peak from west to east manifest the change in air conductivity within the epicentre before the earthquake. For a clearer observation, we have extracted the *TEC* from the GIM-TEC having one-hour temporal resolution, taking the fixed nearest latitude from the epicentre, i.e. 22.5° N and varying longitude ± 20° from the epicentre, i.e. 75° E to 115° E. The variation of the GIM-TEC along the longitude taking latitude of epicentre is studied from 16 March to 1 April. The study is carried out during the EIA active hours, starting from 05:00 to 16:00 UTC (from 11:30 to 22:30 LT). An unusual increase of *TEC* is observed forming the hump in the west from epicentre on 17, 19, 20, and 23 March. The hump is observed to be shifted on the east side on 24 March and no such hump is observed thereafter. It is worthy to mention that the hump was also observed on 22, 26, and 27 March on the western side of the epicentre. As these dates are the geomagnetic D-days, the observed humps are more plausibly linked to the geomagnetic

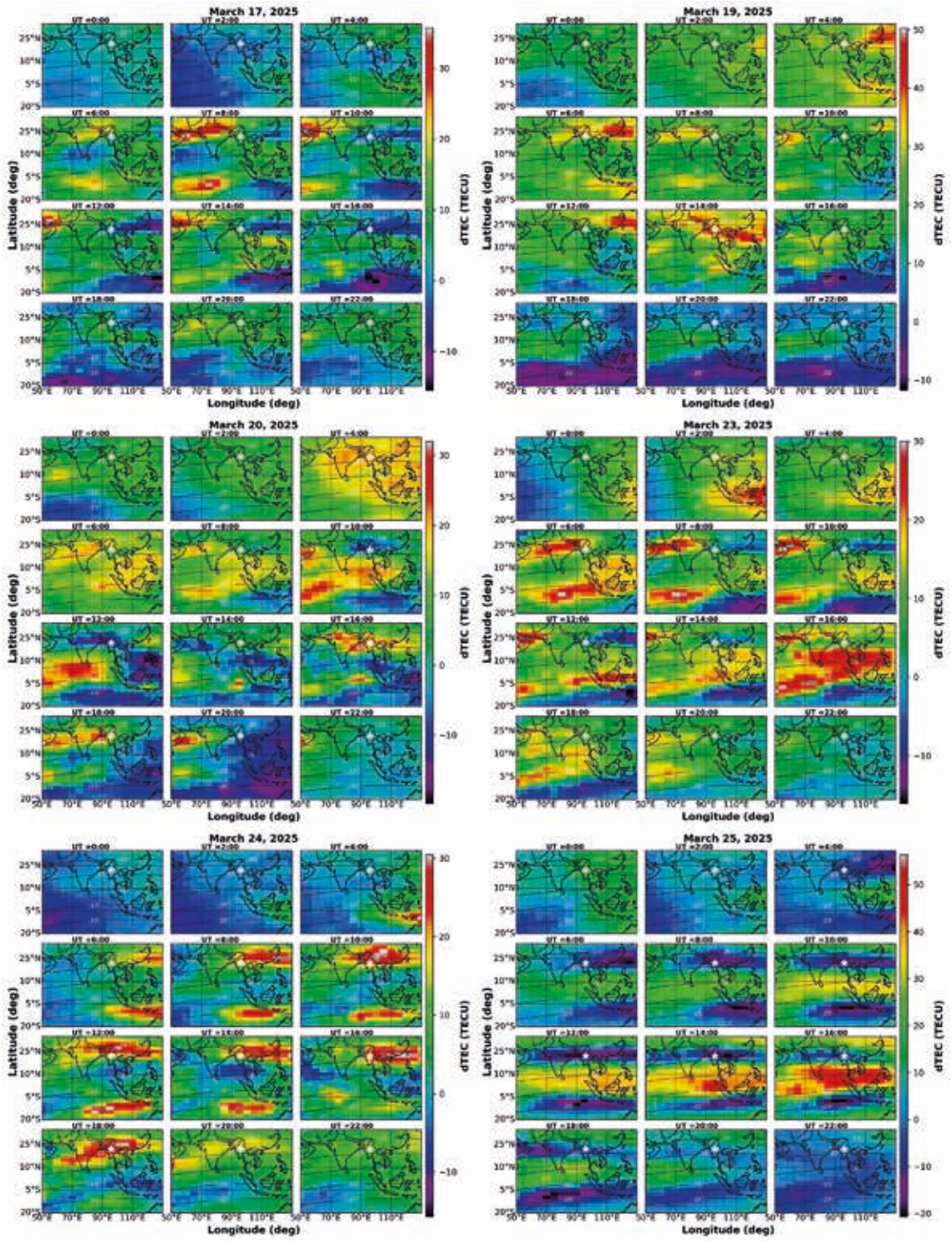


Fig. 6 - The GIM-TEC map of *dTEC* on 17, 19, 20, 23, 24, and 25 March. Each plot consists of sub-plots in the difference of two hours, UTC is given in heading of each subplot, for Myanmar, LT = UTC+6:30. White star represents the epicentre and curve lines represent geomagnetic latitudes; values are marked by white letter. The positive anomaly initially observed west of epicentre on 17 March is shifted to the eastern side of the epicentre by 24 March.

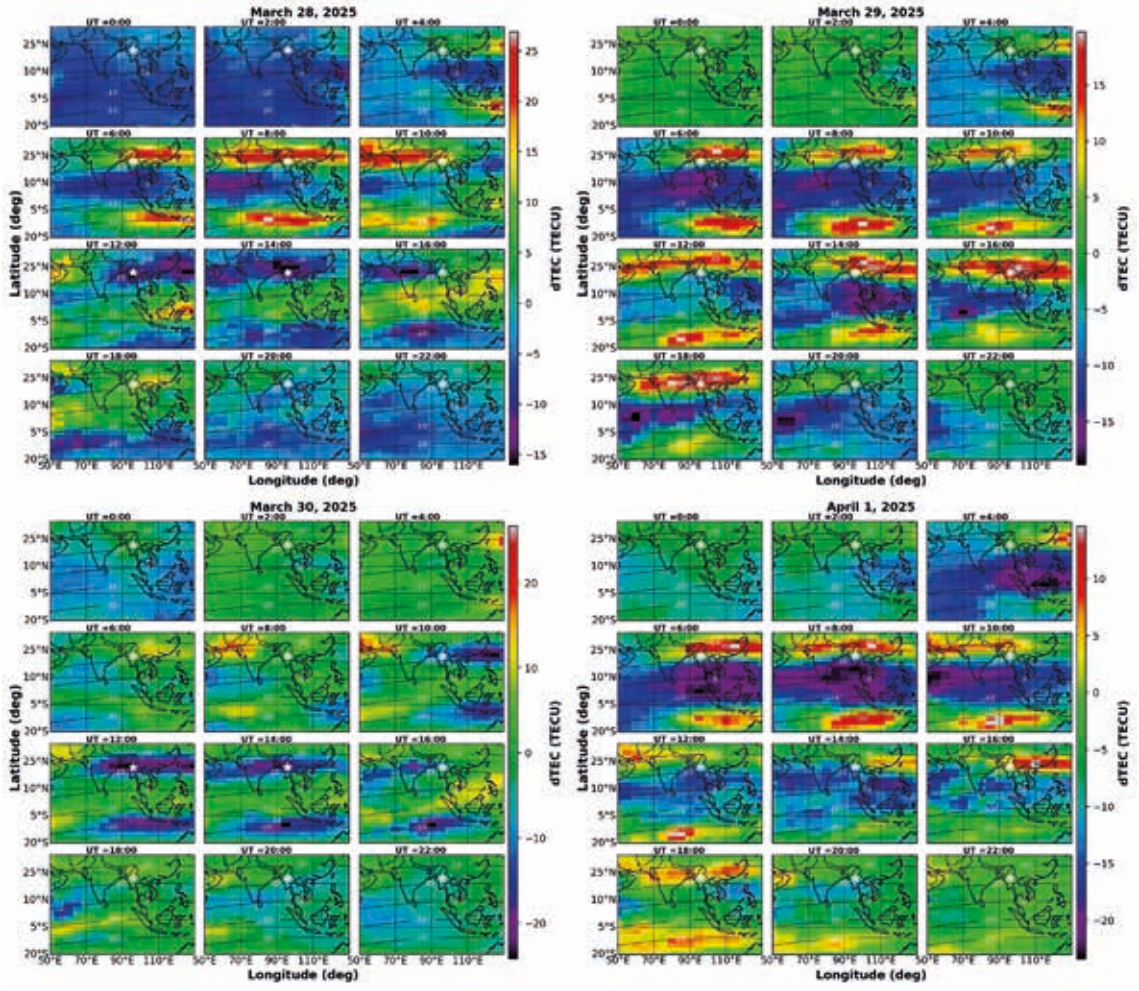


Fig. 7 - The GIM-TEC map of *dTEC* for 28, 29, 30 March, and 1 April. Positive anomaly can be seen nearby the epicentre on 28 and 29 March and 1 April, which agree with *VTEC* data obtained from ground stations.

disturbance rather than to the earthquake. A similar observation was reported during the study of the Wenchuan *M*7.9 earthquake on 12 May 2008 (Pulinets *et al*., 2010; Pulinets, 2012).

The longitudinal variation of the *TEC* on 17, 19, 20, 23, 24, 25, 28, and 29 March at 07:00, 08:00, 14:00, and 16:00 UTC (13:30, 14:30, 20:30, and 22:30 LT) is shown in Fig. 8. The selected hours showing the strongest effects are included, whereas the geomagnetically disturbed days (22, 26, and 27 March) are excluded. These results strongly suggest the changes in atmospheric conductivity near the epicentre prior to the Myanmar *M*7.7 earthquake.

3.4. Dynamics of the EIA near the epicentre

The epicentre of the Myanmar earthquake belongs to the north crest of the EIA region. We studied the variation of the *TEC* on anomaly days along the latitudinal cross section taking fixed longitude of the epicentre 95.936°E, using GIM-TEC data with one-hour temporal resolution. The variation on the EIA trend is compared with the mean value of the five most-disturbed and

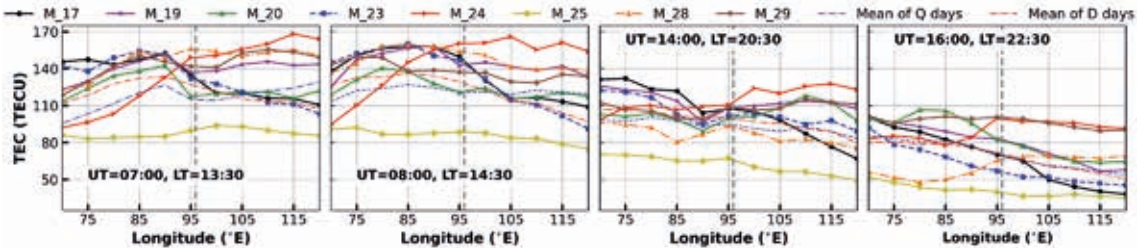


Fig. 8 - Variation of the GIM-TEC along the longitude ±20° east and west from the epicentre of the earthquake at constant latitude 22.5°N. The hours are selected in such a way that the maximum effect can be observed. In legend, M represents March and the vertical grey line represents the longitude of epicentre.

most-quiet days of the corresponding month, shown in Fig. 9. The time is chosen in such a way that the EIA is maximum.

Pulinets (2012) suggested three major effects on the EIA regions due to the modification of the zonal electric field by the anomalous electric field induced by seismic activity, which are distortion in shape of the EIA, movement of the EIA hump towards the geomagnetic equator, and depression on the *TEC* value. All these effects can be seen on 25 March at 09:00 UTC (15:30 LT). On 20 and 23 March the distortion and movement of the EIA crest towards the geomagnetic equator can be noticed. On the days with positive anomalies (16, 24, 28, and 29 March and 1 April), a poleward movement of the EIA crest can be observed. Furthermore, the decrement in

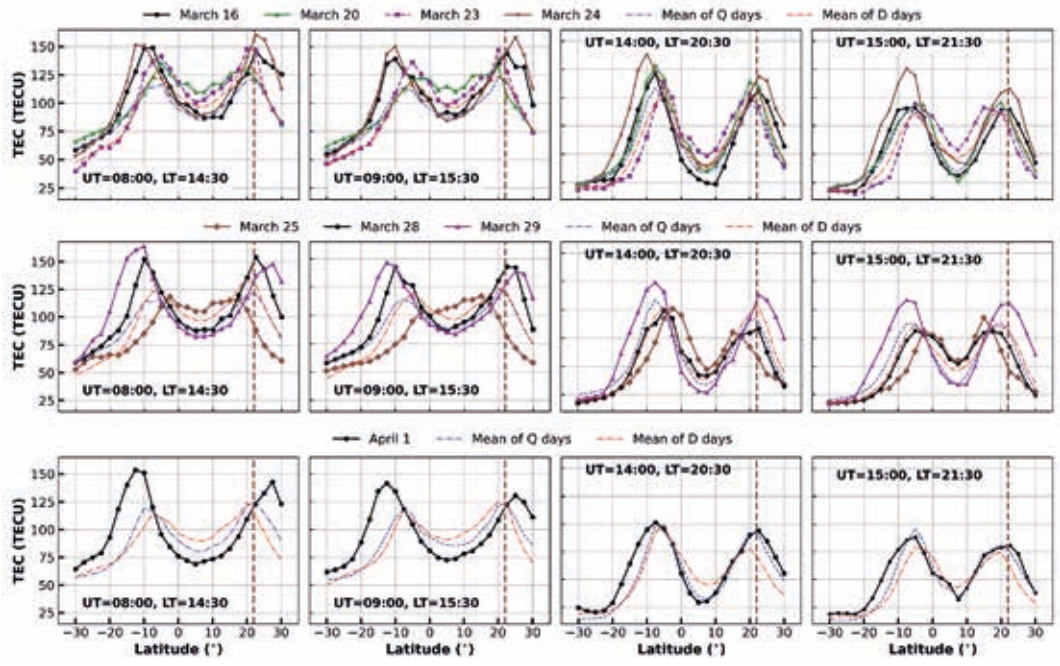


Fig. 9 - Variation of *TEC* along the latitude taking fixed longitude at the epicentre of earthquake (95.936°E) on UTC 08:00, 09:00, 13:00, and 14:00, LT = UTC + 06:30 for Myanmar. The variation of mean value of *TEC* of five most-quiet and most-disturb days of respective month can also be seen. The vertical line represents the latitude of the epicentre (22.011°N).

the *TEC* is observed if the anomaly is negative whereas the enhancement in the *TEC* is observed if the anomaly is positive.

3.5. Discussion

The results obtained from the GNSS ground station and GIM-TEC both indicate the anomaly on the ionospheric *TEC* 12 days before to 4 days after the day of the earthquake. This result can be understood within the LAIC framework based on the radon gas emanation from a few days to a week before the earthquake (Pulinets and Ouzounov, 2011). Radioactive radon gas can ionise the various gaseous molecules in the atmosphere inducing the vertical electric field thereby affecting the GEC. The effect is prominent nearby the epicentre and gradually decreases as the distance increases. The anomalous behaviour of the ionospheric *TEC* was observed only within the EPZ defined by Dobrovolsky *et al.* (1979). Haider *et al.* (2024) also suggested ionospheric *TEC* anomalies seven and six days before the *M*7.8 Turkey earthquake on 6 February 2024 from the GNSS stations within EPZ and no anomalies from GNSS station outside the EPZ in geomagnetic calm conditions. Both negative and positive anomalies in the ionospheric *TEC* were also observed up to a week before the Moroccan *M*6.8 earthquake on 8 September 2023 in geomagnetic calm conditions (Nayak *et al.,* 2023).

The detailed observation of the *dTEC* map obtained from GIM-TEC data explore some behaviour strongly associated with EIA dynamics. The west-to-east shift of the *TEC* anomaly was witnessed from 17 to 24 March. This is another evidence for the reversal of conductivity nearby the epicentre due to the hydration process of the ionised air molecules (Pulinets, 2012). A similar result was also observed in the Wenchuan *M*7.9 earthquake on 12 May 2008 (Pulinets *et al.,* 2010). In the Wenchuan earthquake, the anomaly in the *TEC* shifted from the west of the epicentre to the east after six days and a negative anomaly was observed on the day of the earthquake. In this work, it takes seven days to shift from west to east and negative anomaly is observed three days before the earthquake.

Another important evidence for the seismo-ionospheric coupling mechanism is the morphological change in the EIA profile. On 25 March, the shape of the EIA curve was strongly suppressed and the southern crest nearly disappeared at 09:00 UTC (15:30 LT). Moreover, this effect is also associated with the negative anomaly on the *TEC*, observed from both ground-based GNSS stations and GIM-TEC data. An equatorward movement of the EIA crest was observed on the days with negative anomalies before the earthquake, whereas a poleward movement was observed on the days with positive anomalies before and after the earthquake. Similar results were also observed by Pulinets *et al.* (2010) for the Wenchuan earthquake. The negative anomaly one week before low-latitude earthquakes was also discussed by Liu J.Y. *et al.* (2010). The anomalous electric field that developed prior to the earthquake can modify background eastward zonal electric field, thereby altering the drift. A reduction on the upward drift leads to a simultaneous decrease in intensity and equatorward displacement of the EIA crest.

4. Conclusions

Following are the major conclusions of the study of the ionospheric *TEC* before and after the *M*7.7 Myanmar earthquake on 28 March 2025.

1. The temporal variation of the *VTEC* derived from the GNSS stations within the EPZ suggests anomalies on geomagnetically quiet days, from 12 days before to 4 days after the

earthquake. The GIM-TEC data also show the enhanced *dTEC* values on these anomalous days.

2. The analysis of the *dTEC* map further explores the EIA dynamics. A west-to-east shift of the *TEC* anomaly in the EIA region was observed from 17 to 24 March. This strongly suggests the change in atmospheric conductivity within the epicentre before the earthquake, supporting the seismo-ionospheric coupling mechanism.
3. A modification of the EIA morphology and equatorward shift of the EIA crest were observed three days before the earthquake. These changes coincided with a negative anomaly in both *VTEC* and GIM-TEC data, which is frequently reported in low-latitude earthquakes in previous studies.

These conclusions are based on the study of a single earthquake event. To draw more general conclusions, similar studies should be conducted on additional earthquake events, particularly under geomagnetically quiet conditions to minimise the potential influence of geomagnetic activity. Moreover, the combination of ionospheric *TEC* data with atmospheric and thermal parameters is recommended to provide a comprehensive view of the LAIC mechanism. For future events, incorporating soil radon radioactivity is suggested to examine the consistency and reliability of the observed anomalies.

Acknowledgments. The authors acknowledge the data providers including UNAVCO, NASA (OMNIweb data), IGS, USGS, ISGI whose databases are used in this study, and the developers of open-source software PYTHON and GPS-*TEC*. This work is supported by the University Grants Commission, Nepal, UGC award no.: PhD-81/82-S&T-17.

REFERENCES

Chen Y.I., Chuo J., Liu J.Y. and Pulinets S.A.; 1999: *Statistical study of ionospheric precursors of strong earthquakes at Taiwan area*. In: XXVI URSI General Assembly of the International Union of Radio Science, Toronto, Canada, p.745.

Dobrovolsky I.P., Zubkov S.I. and Miachkin V.I.; 1979: *Estimation of the size of earthquake preparation zones*. Pure Appl. Geophys., 117, 1025-1044, doi: 10.1007/BF00876083.

Ghimire B.D. and Chapagain N.P.; 2022: *Ionospheric anomalies due to Nepal earthquake-2015 as observed from GPS-TEC data*. Geomagn. Aeron., 62, 460-473, doi: 10.1134/S0016793222040041.

Gonzalez W.D., Joselyn J.A., Kamide Y., Kroehl H.W., Rostoker G., Tsurutani B.T. and Vasyliunas V.M.; 1994: *What is a geomagnetic storm?* J. Geophys. Res. Space Phys., 99, 5771-5792, doi: 10.1029/93JA02867.

Haider S.F., Shah M., Li B., Jamjareegulgarn P., de Oliveira-Júnior J.F. and Zhou C.; 2024: *Synchronized and co-located ionospheric and atmospheric anomalies associated with the 2023 Mw 7.8 Turkey earthquake*. Remote Sens., 16, 222, doi: 10.3390/rs16020222.

Hayakawa M.; 2006: *Electromagnetic phenomena associated with earthquakes.* IEEJ Trans. Fundam. Mater., 126, 211-214, doi: 10.1541/ieejfms.126.211.

Hayakawa M.; 2007: *VLF/LF radio sounding of ionospheric perturbations associated with earthquakes*. Sensors, 7, 1141-1158, doi: 10.3390/s7071141.

Hayakawa M. and Molchanov O.A. (eds); 2002: *Seismo electromagnetics: lithosphere-atmosphere-ionosphere coupling.* Terrapub, Tokyo, Japan, 477 pp.

ISGI (International Service of Geomagnetic Indices); n.d.: *Geomagnetic Q-days and D-days.* https://isgi.unistra.fr/data_download.php, accessed May 2025.

Kiyani A., Shah M., Ahmed A., Shah H.H., Hameed S., Adil M.A. and Naqvi N.A.; 2020: *Seismo ionospheric anomalies possibly associated with the 2018 Mw 8.2 Fiji earthquake detected with GNSS TEC.* J. Geodyn., 140, 101782, doi: 10.1016/j.jog.2020.101782.

Le H., Liu J.Y. and Liu L.; 2011: *A statistical analysis of ionospheric anomalies before 736 M6.0+ earthquakes during 2002-2010*. J. Geophys. Res. Space Phys., 116, doi: 10.1029/2010JA015781.

Liu J., Zhang X., Novikov V. and Shen X.; 2016: *Variations of ionospheric plasma at different altitudes before the 2005 Sumatra Indonesia M_s7.2 earthquake*. J. Geophys. Res. Space Phys., 121, 9179-9187, doi: 10.1002/2016JA022758.

Liu J.Y., Tsai H.F. and Jung T.K.; 1996: *Total electron content obtained by using the global positioning system*. Terr. Atmos. Ocean. Sci., 7, 107-117.

Liu J.Y., Chen Y.I., Pulinets S.A., Tsai Y.B. and Chuo Y.J.; 2000: *Seismo-ionospheric signatures prior to M≥6.0 Taiwan earthquakes.* Geophys. Res. Lett., 27, 3113-3116, doi: 10.1029/2000GL011395.

Liu J.Y., Chuo Y.J., Shan S.J., Tsai Y.B., Chen Y.I., Pulinets S.A. and Yu S.B.; 2004: *Pre-earthquake ionospheric anomalies registered by continuous GPS TEC measurements.* Ann. Geophys., 22, 1585-1593, doi: 10.5194/angeo-22-1585-2004.

Liu J.Y., Chen Y.I., Chuo Y.J. and Chen C.S.; 2006: *A statistical investigation of preearthquake ionospheric anomaly.* J. Geophys. Res. Space Phys., 111, doi: 10.1029/2005JA011333.

Liu J.Y., Chen Y.I., Chen C.H., Liu C.Y., Chen C.Y., Nishihashi M., Li J.Z., Xia Y.Q., Oyama K.I., Hattori K. and Lin C.H.; 2009: *Seismoionospheric GPS total electron content anomalies observed before the 12 May 2008 Mw7.9 Wenchuan earthquake*. J. Geophys. Res. Space Phys., 114, doi: 10.1029/2008JA013698.

Liu J.Y., Chen C.H., Chen Y.I., Yang W.H., Oyama K.I. and Kuo K.W.; 2010: *A statistical study of ionospheric earthquake precursors monitored by using equatorial ionization anomaly of GPS TEC in Taiwan during 2001–2007*. J. Asian Earth Sci., 39, 76-80, doi: 10.1016/j.jseaes.2010.02.012.

Nayak K., López-Urías C., Romero-Andrade R., Sharma G., Guzmán-Acevedo G.M. and Trejo-Soto M.E.; 2023: *Ionospheric Total Electron Content (TEC) anomalies as earthquake precursors: unveiling the geophysical connection leading to the 2023 Moroccan 6.8 Mw earthquake*. Geosciences, 13, 319, doi: 10.3390/geosciences13110319.

NASA Space Physics Data Facility; n.d. 1: *Index of /pub/data/gps.* NASA Goddard Space Flight Center. https://spdf.gsfc.nasa.gov/pub/data/gps/, accessed May 2025.

NASA Space Physics Data Facility; n.d. 2: *OMNIWeb.* https://omniweb.gsfc.nasa.gov/form/dx1.html, accessed May 2025.

Neter J., Wasserman W. and Whitmore G.; 1988: *Applied statistics*. *3rd ed.* Allyn and Bacon, Boston, MA, USA, 1006 pp.

Ouzounov D., Bryant N., Logan T., Pulinets S. and Taylor P.; 2006: *Satellite thermal IR phenomena associated with some of the major earthquakes in 1999–2003.* Phys. Chem. Earth, Parts A/B/C, 31, 154-163, doi: 10.1016/j.pce.2006.02.036.

Ouzounov D., Liu D., Chunli K., Cervone G., Kafatos M. and Taylor P.; 2007: *Outgoing long wave radiation variability from IR satellite data prior to major earthquakes*. Tectonophysics, 431, 211-220, doi: 10.1016/j.tecto.2006.05.042.

Pulinets S.; 2012: *Low-latitude atmosphere-ionosphere effects initiated by strong earthquakes preparation process.* Int. J. Geophys., 2012, 131842, doi: 10.1155/2012/131842.

Pulinets S. and Legen'ka A.; 2002: *Dynamics of the near-equatorial ionosphere prior to strong earthquakes.* Geomagn. Aeron., 42, 227-232.

Pulinets S. and Ouzounov D.; 2011: *Lithosphere-Atmosphere-Ionosphere Coupling (LAIC) model - an unified concept for earthquake precursors validation*. J. Asian Earth Sci., 41, 371-382, doi: 10.1016/j.jseaes.2010.03.005.

Pulinets S., Alekseev V., Legen'ka A. and Khegai V.; 1997: *Radon and metallic aerosols emanation before strong earthquakes and their role in atmosphere and ionosphere modification*. Adv. Space Res., 20, 2173-2176, doi: 10.1016/S0273-1177(97)00666-2.

Pulinets S., Alekseev V., Boyarchuk K., Hegai V. and Depuev V.K.; 1999: *Radon and ionosphere monitoring as a means for strong earthquakes forecast*. Nuovo Cimento C, 22, 621-626.

Pulinets S., Gaivoronska T.B., Leyva Contreras A. and Ciraolo L.; 2004: *Correlation analysis technique revealing ionospheric precursors of earthquakes.* Nat. Hazards Earth Syst. Sci., 4, 697-702, doi: 10.5194/nhess-4-697-2004.

Pulinets S., Kotsarenko A., Ciraolo L. and Pulinets I.; 2007: *Special case of ionospheric day-to-day variability associated with earthquake preparation*. Adv. Space Res., 39, 970-977, doi: 10.1016/j.asr.2006.04.032.

Pulinets S., Bondur V., Tsidilina M. and Gaponova M.; 2010: *Verification of the concept of seismoionospheric coupling under quiet heliogeomagnetic conditions, using the Wenchuan (China) earthquake of May 12, 2008, as an example*. Geomagn. Aeron., 50, 231-242, doi: 10.1134/S0016793210020118.

Ryu K., Lee E., Chae J., Parrot M. and Pulinets S.; 2014: *Seismo-ionospheric coupling appearing as equatorial electron density enhancements observed via DEMETER electron density measurements.* J. Geophys. Res. Space Phys., 119(10), 8524-8542, doi: 10.1002/2014JA020284.

Seemala G.K.; n.d.: *GPS-TEC analysis program version 3.5.* https://seemala.blogspot.com/2024/04/gps-tec-analysis-program-version-35.html, accessed May 2025.

Seemala G.K.; 2023: *Estimation of ionospheric total electron content (TEC) from GNSS observations.* In: Singh A.K. and Tiwari S. (eds), Atmospheric Remote Sensing, Elsevier, pp. 63-84, doi: 10.1016/B978-0-323-99262-6.00022-5.

Shah M. and Jin S.; 2018: *Pre-seismic ionospheric anomalies of the 2013 Mw = 7.7 Pakistan earthquake from GPS and COSMIC observations*. Geod. Geodyn., 9, 378-387, doi: 10.1016/j.geog.2017.11.008.

Simha C.P., Natarajan V., Dumka R. and Rao K.M.; 2023: *Spatial and temporal behaviour of Ionospheric VTEC and Atmospheric parameters before New Zealand earthquake on 13th November 2016 (M 7.8)*. J. Appl. Geophys., 212, 104989, doi: 10.1016/j.jappgeo.2023.104989.

Tapping K.F.; 2013: *The 10.7 cm solar radio flux ($F_{10.7}$).* Space Weather, 11, 394-406, doi: 10.1002/swe.20064.

Tariq M.A., Shah M., Hernández-Pajares M. and Iqbal T.; 2019: *Pre-earthquake ionospheric anomalies before three major earthquakes by GPS-TEC and GIM-TEC data during 2015-2017.* Adv. Space Res., 63, 2088-2099, doi: 10.1016/j.asr.2018.12.028.

UNAVCO Inc.; n.d.: *GNSS data.* https://www.unavco.org/data/gps-gnss/gps-gnss.html, accessed May 2025.

USGS (U.S. Geological Survey); n.d.: *Earthquakes.* https://earthquake.usgs.gov/earthquakes/map/, accessed May 2025.

Vincenty T.; 1975: *Direct and inverse solutions of geodesics on the ellipsoid with application of nested equations.* Surv. Rev., 23, 88-93, doi: 10.1179/sre.1975.23.176.88.

Corresponding author: Madhu Sudan Paudel
Department of Physics, Tri-Chandra Multiple Campus, Tribhuvan University
Ghantaghar, Kathmandu, Nepal
Phone: +977 9851283655; e-mails: mspaudel27@gmail.com, madhu.paudel@trc.tu.edu.np